

# Non-Hermitian second-order topological insulator with point gap

Xue-Min Yang<sup>1, 2, 3, 4</sup> Hao Lin,<sup>5</sup> Jian Li,<sup>1, 2, 3, 4</sup> Jia-Ji Zhu,<sup>1, 2, 3, 4</sup> Jun-Li Zhu,<sup>6</sup> and Hong Wu<sup>1, 2, 3, 4, \*</sup>

<sup>1</sup>*School of Electronic Science and Engineering, Chongqing University of Posts and Telecommunications, Chongqing 400065, China*

<sup>2</sup>*Chongqing Key Laboratory of Dedicated Quantum Computing and Quantum Artificial Intelligence, Chongqing 400065, China*

<sup>3</sup>*Key Laboratory of Quantum Artificial Intelligence and New Materials, Chongqing*

<sup>4</sup>*Institute for Advanced Sciences, Chongqing University of Posts and Telecommunications, Chongqing 400065, China*

<sup>5</sup>*School Of Cyber Security and Information Law, Chongqing University of Posts and Telecommunications, Chongqing 400065, China*

<sup>6</sup>*School of Mathematics and Statistics, Chongqing University of Posts and Telecommunications.*

The zero-mode corner states in the gap of two-dimensional non-Hermitian Su-Schrieffer-Heeger model are robust to infinitesimal perturbations that preserve chiral symmetry. However, we demonstrate that this general belief is no longer valid in large-sized systems. To reveal the higher-order topology of non-Hermitian systems, we establish a correspondence between the stable zero-mode singular states and the topologically protected corner states of energy spectrum in the thermodynamic limit. Within this framework, the number of zero-mode singular values is directly linked to the number of mid-gap corner states. The winding numbers in real space can be defined to count the number of stable zero-mode singular states. Our results formulate a bulk-boundary correspondence for both static and Floquet non-Hermitian systems, where topology arises intrinsically from the non-Hermiticity, even without symmetries.

*Introduction.* Topological phases have received extensive attention and developed rapidly due to their potential applications in functional devices[1–4]. The core feature of this type of phase is the existence of protected edge states in the gap [1]. This property can be topologically protected by the symmetries and energy gap of the system. According to the principle of bulk-boundary correspondence, topological invariants can be defined to count the number of boundary states [5].

In recent years, the research of topological insulators has been extended to higher-order cases [6–11]. The  $d$  dimensional higher-order topological insulators of order  $n$  possess  $d - n$  dimensional boundary state, such as corner or hinge states [12–16]. This type of phase is protected by crystalline symmetries. They have been realized in photonic crystal slabs [17], waveguide array [18], electric circuits [19], acoustic crystal [20], and ultracold atoms [21]. On the other hand, non-Hermitian topological phases have also attracted widespread attention [22–34]. A typical feature of such systems is the skin effect with abundant bulk states localized at the edges [35–37]. Therefore, edge states can no longer be characterized by the topological properties of bulk bands, indicating the breakdown of the bulk-boundary correspondence [38]. By replacing the Brillouin zone with the generalized Brillouin zone, topological invariants based on non-Bloch Hamiltonian can be constructed to accurately describe the number of edge states [39–41].

The combination of higher-order topology and non-Hermitian systems has led to the emergence of non-Hermitian higher-order topological insulators [42–44]. The bulk-boundary correspondence has also been studied in these phases. However, under open boundary conditions, the energy spectrum is highly sensitive to perturbations that even maintain symmetry [45–47]. Thus, re-

vealing the non-Hermitian higher-order topology remains a problem.

In this work, we systematically studied static and periodically driven second-order topological insulators. Motivated by the instability of the energy spectrum in finite-sized systems, we establish a correspondence between the number of stable zero-mode singular states and the number of protected topological corner states at the thermodynamic limit energy. The number of corner states in the thermodynamic limit is given by the new topological number instead of the non-Bloch topological number. Our results provide a promising new avenue for exploring novel non-Hermitian topological phases.

*Model and Breakdown of Bulk-Boundary Correspondence.* We consider a two-dimensional (2D) non-Hermitian Su-Schrieffer-Heeger (SSH) model, as illustrated in Fig. 1, where both the  $x$  and  $y$  directions consist of 1D non-Hermitian SSH chains [48]. The non-Hermiticity arises from asymmetric intra-cell hoppings along both directions. This model forms a superlattice with a 4-site unit cell based on a tensor-product structure, where each unit cell can be viewed as the tensor product of 1D dimers along the  $x$  and  $y$  directions, naturally supporting higher-order topological corner states. The Bloch Hamiltonian reads

$$H_{2D}(k_x, k_y) = H_x(k_x) \otimes \mathbb{I}_2 + \mathbb{I}_2 \otimes H_y(k_y), \quad (1)$$

with each 1D block given by

$$\begin{aligned} H_\alpha(k_\alpha) &= \mathbf{h}_\alpha(k_\alpha) \cdot \boldsymbol{\sigma} \\ &= (w_\alpha + v_\alpha \cos k_\alpha) \sigma_x + (v_\alpha \sin k_\alpha + i\gamma_\alpha/2) \sigma_y, \end{aligned} \quad (2)$$

for  $\alpha = x, y$ , where  $v_\alpha$  ( $w_\alpha$ ) denotes the inter-cell (intra-cell) hopping amplitude, and  $\gamma_\alpha$  quantifies the degree of

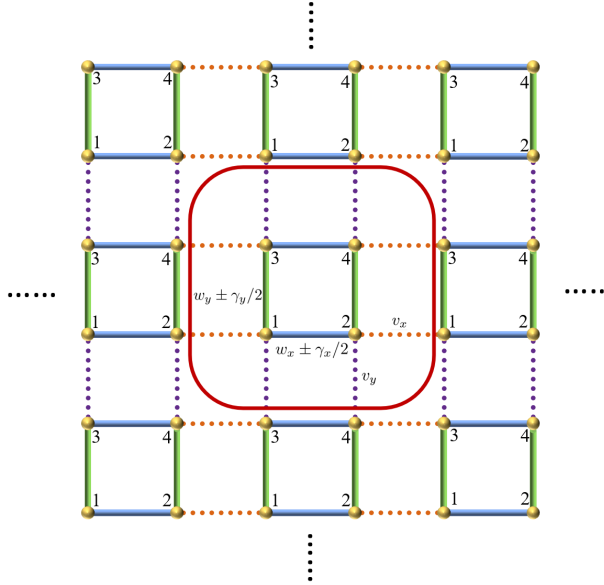


FIG. 1. Schematics of the 2D non-Hermitian Su-Schrieffer-Heeger model on a square lattice. The box indicates the unit cell.

non-Hermitian asymmetry.  $\sigma_{x,y}$  are the Pauli matrices and  $\mathbb{I}_2$  is the  $2 \times 2$  identity matrix.

The eigenvalues of this model are exactly determined as  $E = \varepsilon_x(k_x) + \varepsilon_y(k_y)$ , with  $\varepsilon_\alpha(k_\alpha) = \pm\sqrt{(w_\alpha + v_\alpha \cos k_\alpha)^2 + (v_\alpha \sin k_\alpha + i\gamma_\alpha/2)^2}$ . The 2D eigenstates  $|\psi\rangle_{2D} = |\psi_{k_x}\rangle \otimes |\psi_{k_y}\rangle$  is the tensor product of 1D eigenstates, where  $H_\alpha(k_\alpha)|\psi_{k_\alpha}\rangle = \varepsilon_\alpha(k_\alpha)|\psi_{k_\alpha}\rangle$ . The 2D topological invariant  $\mathcal{V}_{2D} = \mathcal{V}_x \mathcal{V}_y$  is fully determined by two independent 1D winding numbers:

$$\mathcal{V}_\alpha = \frac{1}{2\pi} \frac{[\arg h_\alpha^+ - \arg h_\alpha^-]_{C_{\tilde{k}}}}{2} \in \{0, 1\}, \quad (3)$$

where  $h_\alpha^\pm = h_\alpha^x \pm i h_\alpha^y$  and  $[\arg h_\alpha^\pm]_{C_{\tilde{k}}}$  are the phase changes of  $h_\alpha^\pm$  as  $\tilde{k}$  counterclockwise goes along the generalized Brillouin zone (GBZ)  $C_{\tilde{k}}$ . By replacing the  $k_x, k_y$  with  $k_x - i \ln \sqrt{|\frac{w_x - \gamma_x/2}{w_x + \gamma_x/2}|}$ ,  $k_y - i \ln \sqrt{|\frac{w_y - \gamma_y/2}{w_y + \gamma_y/2}|}$ , we can obtain GBZ. A higher-order topological phase with four protected corner states emerges precisely when  $\mathcal{V}_x = \mathcal{V}_y = 1$ . This model is one of the standard models for investigating non-Hermitian higher-order topology.

As demonstrated in Fig. 2(a), when  $|v_x| > 0.75$ , the smallest  $|E|$  ( $\text{Min}[|E|]$ ) equal to 0 under open boundaries, which is a direct signature of topologically protected corner states. Meanwhile, the bulk winding number  $\mathcal{V}_{2D}$  jumps to 1 at the same critical points, confirming that the bulk topological invariant accurately predicts the boundary phenomenon. This is a manifestation of the bulk-boundary correspondence in higher-order non-Hermitian systems. However, the bulk-boundary correspondence in this non-Hermitian system is highly sensitive to perturbations. As shown in Fig. 2(b), this correspondence can

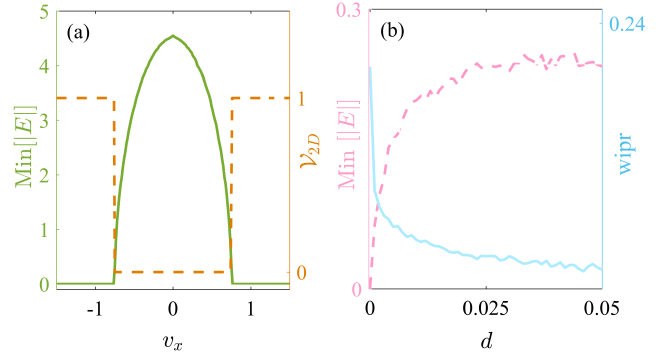


FIG. 2. (a) The minimum modulus of the energy eigenvalues,  $\text{Min}[|E|]$  under open boundary conditions as a function of the horizontal inter-cell hopping amplitude  $v_x$  (green solid curve). The orange dashed curve shows the corresponding winding number  $\mathcal{V}_{2D}$ . The system size is  $1000 \times 1000$  lattice sites, with parameters  $w_x = 1$ ,  $\gamma_x = 1.5$ ,  $w_y = 0$ ,  $\gamma_y = 9$ , and  $v_y = 6v_x$ . When  $|v_x| > 0.75$ , the system enters a higher-order topological phase, signaled by  $\text{Min}[|E|] \rightarrow 0$ , indicating the emergence of topologically protected corner states. (b) The minimum energy modulus (pink dashed curve) and the weighted inverse participation ratio (wipr, sky-blue solid curve) as a function of disorder strength  $d$ . The system size is  $60 \times 60$ , with fixed parameters  $v_x = -1.5$ ,  $w_x = 1$ ,  $\gamma_x = 1.5$ ,  $w_y = 0$ ,  $\gamma_y = 9$ , and  $v_y = -9$ .

still break down even under weak perturbations that preserve chiral symmetry. We add the perturbation term

$$\Delta H = \Delta H_x \otimes \mathbb{I} + \mathbb{I} \otimes \Delta H_y, \quad (4)$$

where  $\Delta H_\alpha = d \left( \kappa_{ij} a_i^\dagger b_j + \kappa_{ji} b_j^\dagger a_i \right)$ , with  $a_i$  ( $b_j$ ) being the annihilation operators on the different sublattice A (B) of the  $i$ th ( $j$ th) unit cell in either the  $x$ - or  $y$ -direction, and  $\kappa_{ij}, \kappa_{ji} \in [-0.5, 0.5]$  are random variables modeling disorder of strength  $d$ . Here,  $\Gamma \Delta H \Gamma^{-1} = -\Delta H$ , with  $\Gamma$  denoting the chiral operator in real space. Even if the strength of disorder is very small, the  $\text{Min}[|E|]$  can deviate significantly from zero (pink dashed curve in Fig. 2(b)). To further view this phenomenon, we introduce the weighted inverse participation ratio (wipr) rather than inverse participation ratio in non-Hermitian systems to describe skin effect. Here, wipr is given by

$$\text{wipr} = \sum_{n,x,y} \frac{|\psi_{n,x,y}|^4}{4L_x L_y} \sqrt{\left(x - \frac{L_x}{2}\right)^2 + \left(y - \frac{L_y}{2}\right)^2}, \quad (5)$$

where  $x, y$  are the lattice site indexes in the  $x$ - and  $y$ -direction, and  $L_x$  ( $L_y$ ) are the length of chains in  $x$  ( $y$ )-direction. It characterizes the extent to which the wavefunction is localized at the boundary. As shown in Fig. 2(b), the wipr (sky-blue solid curve) decreases sharply with disorder strength  $d$ , indicating that the skin effect is highly sensitive to perturbations. Therefore, the energy spectrum in the large-sized systems is unstable. To

explain this, we introduce the condition number

$$\kappa = \|\Sigma\|_2 \|\Sigma^{-1}\|_2, \quad (6)$$

where  $\|\Sigma\|_2$  is the 2-norm of  $\Sigma$  and  $\Sigma$  is a matrix of eigenvectors of Hamiltonian [47]. For the parameters in Fig. 2(b),  $\kappa = 2.93 \times 10^9 \gg 1$  shows that the Hamiltonian is in some sense far from normal. Therefore, the eigenvalues of this non-Hermitian system are highly sensitive to perturbations [47]. The above results demonstrate that the zero-modes can be destroyed by sufficiently weak perturbations, even when chiral symmetry is preserved, proving that these corner states lack topological protection. In this regime, the non-Bloch bulk invariant fails to reliably predict the presence or nature of boundary states, signaling a breakdown of the bulk-boundary correspondence.

*Restoring Bulk-Boundary Correspondence via Singular Value Spectrum.* Given the fact that traditional topological invariants based on the generalized Brillouin zone fail to accurately predict boundary phenomena, a method utilizing the singular value spectrum of the Hamiltonian is proposed to restore the bulk-boundary correspondence. We establish a rigorous connection between the singular value decomposition (SVD) of the non-Hermitian system  $H_{2D} = USV^\dagger$  [49] and the emergence of zero-mode corner states in energy spectrum for the thermodynamic limit. Denoting the column vectors of  $V$  ( $U$ ) by  $v_n$  ( $u_n$ ) and singular values on the diagonal of  $S$  by  $s_n$ , we can obtain

$$H_{2D}^\dagger H_{2D} v_n = s_n^2 v_n. \quad (7)$$

and

$$H_{2D} v_n = s_n u_n. \quad (8)$$

when  $s_n \rightarrow 0$  in the thermodynamic limit, the system supports zero-mode states with wave function  $v_n$ . As shown in Fig. 3(a), the smallest singular value ( $\text{Min}[s]$ ) of the 2D non-Hermitian SSH model is very small for some areas under both clean ( $d = 0$ ) and weakly disordered ( $d = 0.05$ ) conditions. In Fig. 3(b), we demonstrate that such  $\text{Min}[s]$  decays exponentially with increasing system size  $L_x$  or  $L_y$ , confirming the zero-mode singular value in the thermodynamic limit. Besides, these states are all corner states (The inset of Fig. 3(b) shows the probability distribution of one of the zero-mode states). This reveals that the associated eigenstate of  $H_{2D}$  is also spatially localized at the system's corner. Due to the fact that the singular values of  $H_{2D}$  are the square root of eigenvalues of Hermitian operator  $H_{2D}^\dagger H_{2D}$ , they are always real, non-negative, and very stable under weak perturbations [50]. Therefore,  $\text{Min}[s]$  remains insensitive to the disorder strength and size, which is a key feature enabling its use as a stable index to see corner states.

If the non-Hermitian system  $H_{2D}$  has a point gap at  $E = 0$ , we can define a topological invariant via the chiral-symmetric Hermitian matrix [51]

$$\tilde{H} = \begin{pmatrix} 0 & H_{2D} \\ H_{2D}^\dagger & 0 \end{pmatrix}, \quad (9)$$

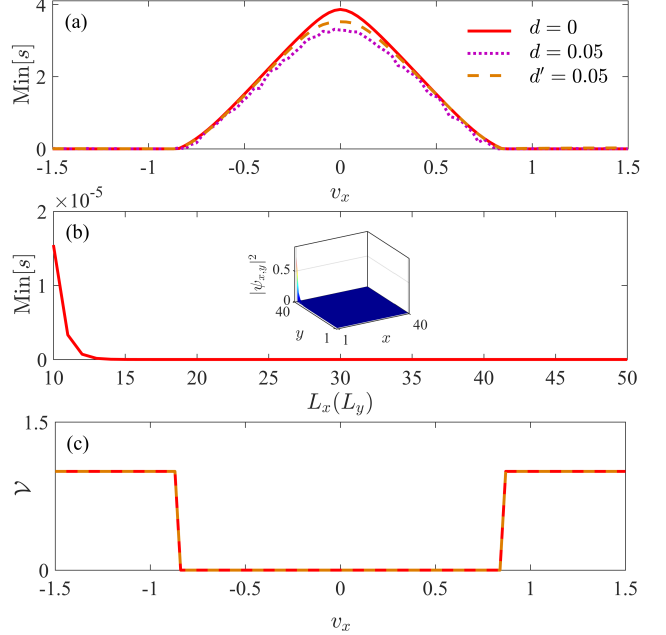


FIG. 3. (a) The smallest singular value ( $\text{Min}[s]$ ) of the 2D non-Hermitian SSH model as a function of the horizontal inter-cell hopping amplitude  $v_x$ . The red solid curve corresponds to the clean system ( $d = 0$ ), while the magenta dashed curve shows the result with weak disorder of strength  $d = 0.05$  that preserves sublattice symmetry; the orange dashed curve represents the case where both  $H_x$  and  $H_y$  are perturbed by a fully random and symmetry-breaking disorder of strength  $d' = 0.05$ . Remarkably, the zero-mode of  $\text{Min}[s]$  persists, indicating that the bulk-boundary correspondence remains intact. (b) Exponential decay of the smallest singular value with increasing system size in either the  $x$ - or  $y$ -direction ( $L_x$  or  $L_y$ ), confirming its correspondence to a zero-mode. The inset displays the spatial probability distribution  $|\psi_{x,y}|^2$  of the associated corner state, localized at the system's corner. (c) Winding number  $\mathcal{V}$  of the bulk Hamiltonian as a function of  $v_x$ . In panels (a) and (c), the system size is  $L_x = L_y = 40$ ; all panels share the same parameters:  $w_x = 1$ ,  $w_y = 0$ ,  $\gamma_x = 1.5$ ,  $\gamma_y = 9$ , and  $v_y = 6v_x$ .

whose eigenvalues are  $\pm s_n$ , where  $s_n$  represents the singular value of  $H_{2D}$ . The winding number  $\mathcal{V}$  of  $\tilde{H}$ , computed as

$$\mathcal{V} = \frac{1}{4\pi i} \text{Tr} \ln(P^A P^{B\dagger}), \quad (10)$$

where  $P^A = U^\dagger P U$ ,  $P^B = V^\dagger P V$ , and

$$P = \text{Diag}[e^{\frac{-i2\pi \times 1 \times 1}{L_x L_y}}, e^{\frac{-i2\pi \times 1 \times 2}{L_x L_y}}, \dots, e^{\frac{-i2\pi \times L_x L_y}{L_x L_y}}] \otimes \mathbb{I}_2. \quad (11)$$

As shown in Fig. 3(c), the position where  $\mathcal{V}$  jumps from 0 to 1 precisely coincides with the location where  $\text{Min}[s]$  becomes zero. The total number of zero-mode singular values equals  $2\mathcal{V}$ , which directly corresponds to the

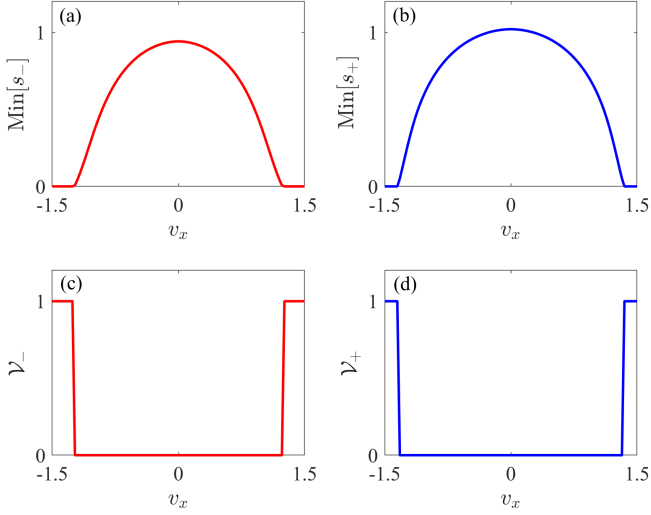


FIG. 4. (a-b) The smallest singular values  $\text{Min}[s_{\mp}]$  of (a)  $U(T) - \mathbb{I}$  and (b)  $U(T) + \mathbb{I}$  as functions of the horizontal inter-cell hopping amplitude  $v_x$ . The zero-mode singular values in (a) and (b) signal the presence of topological 0-mode and  $\pi$ -mode states, respectively. (c-d) Corresponding topological invariants  $\mathcal{V}_-$  and  $\mathcal{V}_+$  as functions of  $v_x$ , which characterize the 0- and  $\pi$ -quasienergy topological phases. Parameters: system size  $L_x = L_y = 40$ ;  $w_x = 1$ ,  $w_y = 0$ ,  $\gamma_x = 1.5$ ,  $\gamma_y = 10.5$ ,  $v_y = 7v_x$ ; full driving period  $T = 0.6$ , the duration of the first segment within each period  $T_1 = 0.3$ , and the intensity ratio factor between the second and the first stage  $q_x = q_y = 0.2$ .

number of topologically protected corner states of energy spectrum in the thermodynamic limit.

To further examine the robustness of our bulk-boundary correspondence, we introduce a fully random and symmetry-breaking weak disorder  $\Delta H' = \Delta H'_x \otimes \mathbb{I} + \mathbb{I} \otimes \Delta H'_y$  to the Hamiltonian. Each matrix element of  $\Delta H'_\alpha$  is drawn independently and uniformly from the interval  $[-d', d']$ . Remarkably, despite the introduction of a fully random, symmetry-breaking disorder, the bulk-boundary correspondence remains intact. As shown in Fig. 3(a), the smallest singular value  $\text{Min}[s]$  is also equal to zero in the topologically nontrivial regime, and the number of zero-mode singular values exactly matches the bulk winding number  $2\mathcal{V}$ . This demonstrates that the singular-value-based topological characterization is robust against perturbations that would otherwise destabilize conventional bulk-boundary correspondence. Our framework thus provides a stable and reliable route to identify topological boundary states in non-Hermitian systems, even in the absence of chiral symmetry.

*Extension to Floquet Non-Hermitian Systems.* The method used to establish bulk-boundary correspondence in static system can be generalized to periodically driven non-Hermitian systems. We consider a Floquet 2D Non-Hermitian SSH model with time-periodic hopping ampli-

tudes:

$$v_\alpha(t) = \begin{cases} f_\alpha, & t \in [mT, mT + T_1) \\ q_\alpha f_\alpha, & t \in [mT + T_1, (m+1)T) \end{cases}, \quad (12)$$

where  $T$  is the driving period,  $m \in \mathbb{Z}$ ,  $T_1$  is the duration of the first segment, and  $q_\alpha$  controls the amplitude ratio between different segments. This system lacks a well defined energy spectrum. According to Floquet theorem, the one-period evolution operator  $U(T) = \mathbb{T}e^{-i \int_0^T H(t) dt}$  can be used to define an effective Hamiltonian

$$H_{\text{eff}} = \frac{i}{T} \ln[U(T)] = H_{\text{eff},x} \otimes \mathbb{I} + \mathbb{I} \otimes H_{\text{eff},y}, \quad (13)$$

where

$$H_{\text{eff},\alpha} = \frac{i}{T} \ln[e^{-iH_2(k_\alpha)T_2} e^{-iH_1(k_\alpha)T_1}] \quad (\alpha = x, y), \quad (14)$$

and  $T_2 = T - T_1$ . Eigenvalues of the effective Hamiltonian  $H_{\text{eff}}$  lie on the  $\varepsilon_j \in [-\pi/T, \pi/T]$  and constitute the quasienergy spectrum of the system[52]. Topological phase of periodically driven system are defined in such quasienergy spectrum [52–58].

To characterize topology in this setting, we introduce two auxiliary operators:  $U(T) - \mathbb{I}$  and  $U(T) + \mathbb{I}$ , whose singular values directly probe the presence of 0-mode and  $\pi$ -mode states, respectively. As shown in Figs. 4(a,b), the smallest singular values  $\text{Min}[s_{\mp}]$  of these operators  $U(T) \mp \mathbb{I}$  equal to zero, signaling the emergence of topologically protected 0- and  $\pi$ -modes under open boundaries. Crucially, unlike the complex quasienergy spectrum, these singular values remain robust against disorder and insensitive to boundary conditions, which is a key advantage for practical characterization.

We further define two topological invariants,  $\mathcal{V}_+$  and  $\mathcal{V}_-$ , based on the winding numbers of

$$\tilde{H}'_{\pm} = \begin{pmatrix} 0 & U(T) \pm \mathbb{I} \\ U(T)^\dagger \pm \mathbb{I} & 0 \end{pmatrix}, \quad (15)$$

which are computed as

$$\mathcal{V}_\pm = \frac{1}{4\pi i} \text{Tr} \ln(P_\pm^A P_\pm^{B\dagger}), \quad (16)$$

where  $U(T) \pm \mathbb{I} = U_\pm S'_\pm V_\pm^\dagger$ ,  $P_\pm^A = U_\pm^\dagger P U_\pm$ ,  $P_\pm^B = V_\pm^\dagger P V_\pm$ , and  $P$  is defined in Eq.(11). As depicted in Figs. 4(c,d), the zero-mode singular value can be well characterized by the topological invariants. The number of zero-mode singular values equals  $2\mathcal{V}_-$  (for 0-modes) and  $2\mathcal{V}_+$  (for  $\pi$ -modes), providing a direct count of topologically protected corner states. By analyzing the singular value spectrum of simple Hermitian operators  $\tilde{H}'_{\pm}$  derived from  $U(T)$ , we obtain a new method to classify Floquet topological phases.

*Discussion and Conclusion.* In summary, we investigated the higher-order topology of static and Floquet

non-Hermitian SSH model. With the help of singular value spectrum, we demonstrate that the zero-mode singular value robustly signals the emergence of topologically protected corner states of energy spectrum in the thermodynamic limit, even in the absence of chiral symmetry. The winding numbers in real space can be defined to count the number of stable zero-mode singular states. We have established a unified framework to restore the bulk-boundary correspondence in non-Hermitian higher-order topological phases, both in static and Floquet systems.

In recent years, non-Hermitian Hamiltonian has been realized in photonic quantum walks [59], Photonic Quasicrystal [60], cold Rydberg quantum gases [61], and waveguides [62]. Floquet higher-order topological phases has been observed in acoustic lattice [63] and Rydberg atoms [64]. Based on these developments, we believe that our approach is experimentally feasible.

*Acknowledgments.* This work is supported by National Natural Science Foundation (Grants No. 12405007 and NO. 12305011), Funds for Young Scientists of Chongqing Municipal Education Commission(Grant No. KJQN202400603 and NO. KJQN202500619), Natural Science Foundation of Chongqing (Grant No. CSTB2025NSCQ-GPX1265, No. CSTB2022NSCQ-MSX0316, CSTB2024NSCQ-MSX0736, and CSTB2025NSCQ-GPX1315), and Chongqing Natural Science Foundation Project (Grant No. CSTB2025NSCQ-LZX0142)

disorder-induced second-order topological insulators in three dimensions, *Phys. Rev. Lett.* **126**, 206404 (2021).

- [10] L. Trifunovic and P. W. Brouwer, Higher-order bulk-boundary correspondence for topological crystalline phases, *Phys. Rev. X* **9**, 011012 (2019).
- [11] R. Chen, C.-Z. Chen, J.-H. Gao, B. Zhou, and D.-H. Xu, Higher-order topological insulators in quasicrystals, *Phys. Rev. Lett.* **124**, 036803 (2020).
- [12] F. Schindler, A. M. Cook, M. G. Vergniory, Z. Wang, S. S. P. Parkin, B. A. Bernevig, and T. Neupert, Higher-order topological insulators, *Science Advances* **4**, eaat0346 (2018).
- [13] C. Chen, L. Qi, Y. Xing, W.-X. Cui, S. Zhang, and H.-F. Wang, General bounded corner states in two-dimensional off-diagonal Aubry–André–Harper model with flat bands, *New Journal of Physics* **23**, 123008 (2021).
- [14] Z. Xiong, Y. Liu, Z.-K. Lin, Z.-L. Kong, and J.-H. Jiang, Triband higher-order topological insulators, *Phys. Rev. Appl.* **24**, 024049 (2025).
- [15] J. Xiao, Q. Hu, Z. Yu, W. Chen, and X. Luo, Magnetic flux induced higher-order topological superconductivity, *Phys. Rev. B* **112**, 195404 (2025).
- [16] W. Jia, Y. Tian, H. Yang, X. Kong, Z.-H. Huang, W.-J. Gong, and J.-H. An, Unconventional hybrid-order topological insulators, *Phys. Rev. B* **112**, L241103 (2025).
- [17] X.-D. Chen, W.-M. Deng, F.-L. Shi, F.-L. Zhao, M. Chen, and J.-W. Dong, Direct observation of corner states in second-order topological photonic crystal slabs, *Phys. Rev. Lett.* **122**, 233902 (2019).
- [18] A. Cerjan, M. Jürgensen, W. A. Benalcazar, S. Mukherjee, and M. C. Rechtsman, Observation of a higher-order topological bound state in the continuum, *Phys. Rev. Lett.* **125**, 213901 (2020).
- [19] W. Zhang, D. Zou, Q. Pei, W. He, J. Bao, H. Sun, and X. Zhang, Experimental observation of higher-order topological Anderson insulators, *Phys. Rev. Lett.* **126**, 146802 (2021).
- [20] D. Wang, Y. Deng, J. Ji, M. Oudich, W. A. Benalcazar, G. Ma, and Y. Jing, Realization of a  $\mathbb{Z}$ -classified chiral-symmetric higher-order topological insulator in a coupling-inverted acoustic crystal, *Phys. Rev. Lett.* **131**, 157201 (2023).
- [21] Z. Dong, H. Li, H. Wang, Y. Pan, W. Yi, and B. Yan, Observation of higher-order topological bound states in the continuum using ultracold atoms (2025), arXiv:2501.13499 [cond-mat.quant-gas].
- [22] K. Kawabata, K. Shiozaki, M. Ueda, and M. Sato, Symmetry and topology in non-Hermitian physics, *Phys. Rev. X* **9**, 041015 (2019).
- [23] K. Bai, J.-Z. Li, T.-R. Liu, L. Fang, D. Wan, and M. Xiao, Nonlinear exceptional points with a complete basis in dynamics, *Phys. Rev. Lett.* **130**, 266901 (2023).
- [24] M. Jangjan, L. Li, L. E. F. Foa Torres, and M. V. Hosseini, Topological phases of commensurate or incommensurate non-Hermitian Su-Schrieffer-Heeger lattices, *Phys. Rev. B* **109**, 205142 (2024).
- [25] J. Y. Lee, J. Ahn, H. Zhou, and A. Vishwanath, Topological correspondence between Hermitian and non-Hermitian systems: Anomalous dynamics, *Phys. Rev. Lett.* **123**, 206404 (2019).
- [26] C.-X. Guo, S. Chen, K. Ding, and H. Hu, Exceptional non-Abelian topology in multiband non-Hermitian systems, *Phys. Rev. Lett.* **130**, 157201 (2023).
- [27] L. Jezequel and P. Delplace, Non-Hermitian spectral

\* Contact author: wuh@cqupt.edu.cn

- [1] M. Z. Hasan and C. L. Kane, Colloquium: Topological insulators, *Rev. Mod. Phys.* **82**, 3045 (2010).
- [2] T. Ozawa, H. M. Price, A. Amo, N. Goldman, M. Hafezi, L. Lu, M. C. Rechtsman, D. Schuster, J. Simon, O. Zilberman, and I. Carusotto, Topological photonics, *Rev. Mod. Phys.* **91**, 015006 (2019).
- [3] N. R. Cooper, J. Dalibard, and I. B. Spielman, Topological bands for ultracold atoms, *Rev. Mod. Phys.* **91**, 015005 (2019).
- [4] B. Q. Lv, T. Qian, and H. Ding, Experimental perspective on three-dimensional topological semimetals, *Rev. Mod. Phys.* **93**, 025002 (2021).
- [5] C.-K. Chiu, J. C. Y. Teo, A. P. Schnyder, and S. Ryu, Classification of topological quantum matter with symmetries, *Rev. Mod. Phys.* **88**, 035005 (2016).
- [6] W. A. Benalcazar, B. A. Bernevig, and T. L. Hughes, Quantized electric multipole insulators, *Science* **357**, 61–66 (2017).
- [7] F. Liu and K. Wakabayashi, Novel topological phase with a zero Berry curvature, *Phys. Rev. Lett.* **118**, 076803 (2017).
- [8] M. Ezawa, Topological switch between second-order topological insulators and topological crystalline insulators, *Phys. Rev. Lett.* **121**, 116801 (2018).
- [9] J.-H. Wang, Y.-B. Yang, N. Dai, and Y. Xu, Structural-

flows and Berry-Chern monopoles, *Phys. Rev. Lett.* **130**, 066601 (2023).

[28] M.-W. Li, J.-W. Liu, X. Wang, W.-J. Chen, G. Ma, and J.-W. Dong, Topological temporal boundary states in a non-Hermitian spatial crystal, *Phys. Rev. Lett.* **135**, 187101 (2025).

[29] K.-X. Hu, C. Luo, J. Zhang, S. Liu, W.-X. Cui, J. Cao, S. Zhang, and H.-F. Wang, Bulk-boundary correspondence in non-Hermitian class-d<sup>†</sup> topological systems, *Phys. Rev. A* **112**, 052209 (2025).

[30] M. Zhang, Y. Zhang, S. Li, Y.-a. Li, Y. Wei, R. Tian, T. Wu, H. Shi, H. Gao, F. Li, and B. Liu, Observation of non-Hermitian bulk-boundary correspondence in nonchiral nonunitary quantum dynamics of single photons, *Phys. Rev. Lett.* **135**, 213601 (2025).

[31] E. Ma, K. Zhang, and Z. Song, Dynamically stable topological edge states in an extended Su-Schrieffer-Heeger ladder with balanced perturbation, *Phys. Rev. B* **112**, 195134 (2025).

[32] H. Wu and L. Jin, Topological zero modes from the interplay of  $\mathcal{PT}$  symmetry and anti- $\mathcal{PT}$  symmetry, *Phys. Rev. B* **112**, 125146 (2025).

[33] C. Yuce and H. Ramezani, Topological states in a non-Hermitian two-dimensional Su-Schrieffer-Heeger model, *Phys. Rev. A* **100**, 032102 (2019).

[34] S. A. A. Ghorashi and M. Sato, Topological reality switch: Towards bulk-boundary selective lasing (2025), arXiv:2507.02038 [quant-ph].

[35] S. Longhi, Erratic non-Hermitian skin localization, *Phys. Rev. Lett.* **134**, 196302 (2025).

[36] K. Zhang, Z. Yang, and K. Sun, Edge theory of non-Hermitian skin modes in higher dimensions, *Phys. Rev. B* **109**, 165127 (2024).

[37] J. Shi and A. N. Poddubny, Chiral dissociation of bound photon pairs for a non-Hermitian skin effect, *Phys. Rev. Lett.* **134**, 233602 (2025).

[38] T. E. Lee, Anomalous edge state in a non-Hermitian lattice, *Phys. Rev. Lett.* **116**, 133903 (2016).

[39] S. Yao and Z. Wang, Edge states and topological invariants of non-Hermitian systems, *Phys. Rev. Lett.* **121**, 086803 (2018).

[40] K. Yokomizo and S. Murakami, Non-Bloch band theory of non-Hermitian systems, *Phys. Rev. Lett.* **123**, 066404 (2019).

[41] H. Wu and J.-H. An, Floquet topological phases of non-Hermitian systems, *Phys. Rev. B* **102**, 041119 (2020).

[42] T. Liu, Y.-R. Zhang, Q. Ai, Z. Gong, K. Kawabata, M. Ueda, and F. Nori, Second-order topological phases in non-Hermitian systems, *Phys. Rev. Lett.* **122**, 076801 (2019).

[43] Z. Zhang, M. Rosendo López, Y. Cheng, X. Liu, and J. Christensen, Non-Hermitian sonic second-order topological insulator, *Phys. Rev. Lett.* **122**, 195501 (2019).

[44] J. Pan and L. Zhou, Non-Hermitian Floquet second order topological insulators in periodically quenched lattices, *Phys. Rev. B* **102**, 094305 (2020).

[45] K. Monkman and J. Sirker, Hidden zero modes and topology of multiband non-Hermitian systems, *Phys. Rev. Lett.* **134**, 056601 (2025).

[46] H. Wu, X.-M. Yang, and H. Liu, Breakdown of non-Bloch bulk-boundary correspondence and emergent topology in Floquet non-Hermitian systems (2025), arXiv:2510.09193 [quant-ph].

[47] L. N. Trefethen and M. Embree, *Spectra and Pseudospectra* (Princeton University Press, 2005).

[48] Y. Jing, J.-J. Dong, Y.-Y. Zhang, and Z.-X. Hu, Biorthogonal dynamical quantum phase transitions in non-Hermitian systems, *Phys. Rev. Lett.* **132**, 220402 (2024).

[49] L. Herviou, J. H. Bardarson, and N. Regnault, Defining a bulk-edge correspondence for non-Hermitian hamiltonians via singular-value decomposition, *Phys. Rev. A* **99**, 052118 (2019).

[50] Y. Ashida, Z. Gong, and M. Ueda, Non-hermitian physics, *Advances in Physics* **69**, 249–435 (2020).

[51] W. A. Benalcazar and A. Cerjan, Chiral-symmetric higher-order topological phases of matter, *Phys. Rev. Lett.* **128**, 127601 (2022).

[52] A. Kundu, H. A. Fertig, and B. Seradjeh, Effective theory of Floquet topological transitions, *Phys. Rev. Lett.* **113**, 236803 (2014).

[53] P. M. Perez-Piskunow, G. Usaj, C. A. Balseiro, and L. E. F. F. Torres, Floquet chiral edge states in graphene, *Phys. Rev. B* **89**, 121401 (2014).

[54] R. Roy and F. Harper, Periodic table for Floquet topological insulators, *Phys. Rev. B* **96**, 155118 (2017).

[55] Y. T. Katan and D. Podolsky, Modulated Floquet topological insulators, *Phys. Rev. Lett.* **110**, 016802 (2013).

[56] S.-Y. Bai, C. Chen, H. Wu, and J.-H. An, Quantum control in open and periodically driven systems, *Advances in Physics: X* **6**, 1870559 (2021).

[57] M. Ghuneim and R. W. Bomantara, Anomalous topological edge modes in a periodically driven trimer lattice, *Phys. Rev. B* **111**, 195424 (2025).

[58] G. K. Dash, S. Bid, and M. Thakurathi, Floquet exceptional topological insulator, *Phys. Rev. B* **109**, 035418 (2024).

[59] L. Xiao, W.-T. Xue, F. Song, Y.-M. Hu, W. Yi, Z. Wang, and P. Xue, Observation of non-Hermitian edge burst in quantum dynamics, *Phys. Rev. Lett.* **133**, 070801 (2024).

[60] Z. Zhang, S. Liang, I. Septembre, J. Yu, Y. Huang, M. Liu, Y. Zhang, M. Xiao, G. Malpuech, and D. Solnyshkov, Non-Hermitian delocalization in a two-dimensional photonic quasicrystal, *Phys. Rev. Lett.* **132**, 263801 (2024).

[61] J. Zhang, Y.-J. Wang, S.-Y. Shao, B. Liu, L.-H. Zhang, Z.-Y. Zhang, X. Liu, C. Yu, Q. Li, H.-C. Chen, Y. Ma, T.-Y. Han, Q.-F. Wang, J.-D. Nan, Y.-M. Yin, D.-Y. Zhu, Q.-Q. Fang, D.-S. Ding, and B.-S. Shi, Observation of non-Hermitian topology in cold Rydberg quantum gases (2025), arXiv:2509.26256 [cond-mat.quant-gas].

[62] Z. Lin, J. Li, W. Song, S. Su, J. Sun, S. Wu, C. Huang, S. Zhu, and T. Li, Dissipative topological dynamics in optical waveguides: Sensitivity versus robustness, *Phys. Rev. Lett.* **134**, 223802 (2025).

[63] W. Zhu, H. Xue, J. Gong, Y. Chong, and B. Zhang, Time-periodic corner states from Floquet higher-order topology, *Nature Communications* **13**, 11 (2022).

[64] S.-Y. Shao, Q. Li, H.-C. Chen, B.-S. Shi, and D.-S. Ding, Higher-order and fractional discrete time crystals in floquet-driven rydberg atoms, *Nature Communications* **17**, 9730 (2024).